Applied Physics A (2018) 124:656
https://doi.org/10.1007/s00339-018-2083-6

Applied Physics A
Materials Science & Processing

Phonon-assisted cyclotron resonance in special symmetric quantum wells

Khang D. Pham[1,2] · Nguyen N. Hieu[3] · Le T. T. Phuong[4] · Bui D. Hoi[4] · Chuong V. Nguyen[5] · Huynh V. Phuc[6]

Received: 26 June 2018 / Accepted: 30 August 2018

Abstract
In this work, the phonon-assisted cyclotron resonance in a special symmetric quantum well is studied in detail by evaluating the magneto-optical absorption coefficient (MOAC) and the full width at half maximum (FWHM). The results include the two-photon absorption process and the electron–phonon interaction as well. The influence of the magnetic field, the quantum well parameter, and the temperature on the MOAC and the FWHM is illustrated plainly. Our results are in good agreement with those accessible to the theoretical and experimental works of literature. In addition, we found a new rule of the temperature-dependent FWHM for the phonon absorption process, which should be examined by an experiment work in the future.

1 Introduction

The resonance effects are known to be a powerful technique that can be used to investigate the scattering mechanisms of electrons in low-dimensional semiconductor systems. Up to date, there are many types of the resonance effects recognized in the literature such as electro-phonon resonance [1–4], cyclotron resonance (CR) [5–7], and magneto-phonon resonance [8–10], in which the magnetic field is present in the latter but absent in the former. In the cyclotron resonance case, the resonant peaks appear at the positions given by the relation $\hbar\Omega = p\hbar\omega_B$, where $\hbar\Omega$ and $\hbar\omega_B$ are the photon energy and cyclotron energy, respectively, and p is a positive integer. In this effect, electrons absorb photon energy to transfer between Landau levels (LL) without scattering with phonon. The CR effect has been recognized to be a powerful tool for measuring the effective mass of electrons in semiconductors [11]. In an experiment, CR is usually used to examine the kinetic coefficients of bulk solids [12] and two-dimensional semiconductor structures as well [13]. However, the lack of the electron–phonon (e–p) scattering in the model of this effect prevents its application from investigating the absorption processes occurring at other values of photon energies which satisfies the above condition.

The e–p interaction has been confirmed to have a powerful influence on the transport properties of low-dimensional semiconductor systems [14–16]. When the e–p scattering is included, instead of the simple condition $\hbar\Omega = p\hbar\omega_B$, the resonant condition now reads as $\hbar\Omega = p\hbar\omega_B \pm \hbar\omega_L$, where $\hbar\omega_L$ is the LO-phonon energy. This formula describes another resonant effect, called the magneto-phonon resonance or the phonon-assisted cyclotron resonance (PACR) as used in this paper. In comparison with the CR, it is clear that the PACR effect is more powerful. That is the reason why the PACR has received the substantial attention of researchers in the recent years [17–22]. The results from these works showed that the magnetic field, the temperature, and the systems' size have significant influence not only on the position but also the intensity of the PACR peaks. The limitation of

✉ Huynh V. Phuc
hvphuc@dthu.edu.vn

Khang D. Pham
phamdinhkhang@tdt.edu.vn

[1] Theoretical Physics Research Group, Advanced Institute of Materials Science, Ton Duc Thang University, Ho Chi Minh, Viet Nam

[2] Faculty of Applied Sciences, Ton Duc Thang University, Ho Chi Minh, Vietnam

[3] Institute of Research and Development, Duy Tan University, Da Nang 550000, Vietnam

[4] Physics Department, University of Education, Hue University, Hue 530000, Vietnam

[5] Department of Materials Science and Engineering, Le Quy Don Technical University, Hanoi 100000, Vietnam

[6] Division of Theoretical Physics, Dong Thap University, Cao Lãnh, Dong Thap 870000, Vietnam

Published online: 01 September 2018

these works is that the effect of these parameters on the full width at half maximum (FWHM) of the PACR peaks has still not been properly considered.

Because of having a direct relationship with the e–p interaction, especially in the broadening Landau level mechanism [23], the FWHM has been signified to be a valuable parameter to survey the role of the e–p interaction not only in low-dimensional semiconductor systems [24–26] but also in new types of materials such as graphene [27–31] and monolayer molybdenum disulfide [32]. These results showed that the FWHM strongly varies with the change of magnetic field and structural characteristics in all types of materials. However, the temperature-dependent FWHM is used to distinguish between different elements. While increasing significantly in conventional low-dimensional semiconductor systems and monolayer molybdenum disulfide, the FWHM in graphene is almost independent from the temperature variation.

In this work, we discuss the PARC in a special symmetric quantum well (SSQW) via evaluating the magneto-optical absorption coefficient (MOAC) and the FWHM as well. The MOAC expression is obtained by the perturbative theory [32] in which the e–p interaction is included, while the FWHM is probed by the profile method [33]. The variation of MOAC and FWHM under the influence of magnetic field, quantum well parameter, and temperature are showed and discussed explicitly. In Sect. 2, we briefly display the investigated quantum well model. Section 3 presents the PACR effect in which the MOAC expression is shown in details. Our numerical results are discussed in Sect. 4. Finally, the conclusion is displayed in Sect. 5.

2 Quantum well characteristics

We consider the Hamiltonian of a single electron in SSQW

$$\mathcal{H} = \frac{1}{2m^*}(\mathbf{p} + e\mathbf{A})^2 + U(z), \tag{1}$$

where the Landau gauge is employed for the vector potential $\mathbf{A} = (0, Bx, 0)$, in which the magnetic field B is applied to the z direction (perpendicular to the barriers of quantum well). The spherical electron effective mass $m^* = 0.067m_0$ with m_0 being the rest of the electron mass [34] is used for the reason of convenience. In Eq. (1), the confining potential, $U(z)$, is given by [35]

$$U(z) = U_0 \cot^2 \frac{\pi z}{a}, \ 0 < z < a, \tag{2}$$

where U_0 and a are the modifiable parameters describing the properties of the confinement potential. In Fig. 1, we illustrate the quantum well shapes for several values of a. It is observed that the axis of symmetry of the quantum well shifts towards the right side with the larger values of a parameter.

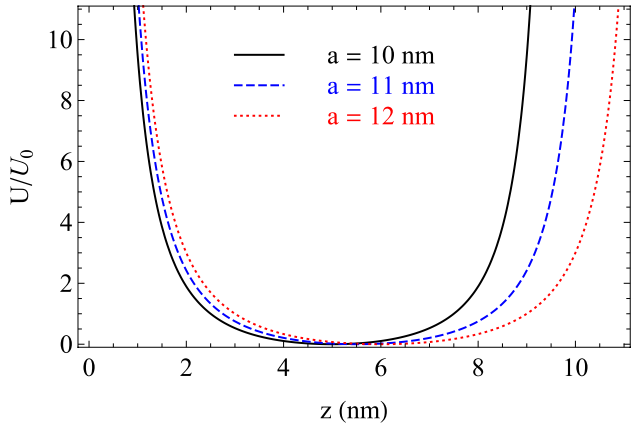

Fig. 1 Quantum well potential for several values of a parameter

The electron eigenstates $|\lambda\rangle$ and eigenvalues $E_{N,n}$ corresponding to the Hamiltonian (1) are given as follows [21, 22]

$$|\lambda\rangle = |N, n, k_y\rangle = \frac{e^{ik_y y}}{\sqrt{L_y}} \psi_N(x - x_0)\phi_n(z), \tag{3}$$

$$E_\lambda \equiv E_{N,n} = \left(N + \frac{1}{2}\right)\hbar\omega_B + \varepsilon_n, \tag{4}$$

where the natural number $N = 0, 1, 2, \ldots$ presents the LL index, k_y and L_y are, respectively, the wave vector of electron and the normalization length in the y direction. The cyclotron frequency is $\omega_B = eB/m^*$, and $\psi_N(x - x_0)$ presents the harmonic oscillator functions, which has the center at $x_0 = -\hbar k_y/m^*\omega_B$. The z component eigenstates in Eq. (3) are as follows [35]

$$\phi_n(z) = c_n \left(\sin \frac{\pi z}{a}\right)^{-2\beta} {}_2F_1\left(-\frac{n}{2} - 2\beta, \frac{n}{2}, \frac{1}{2}, \cos^2 \frac{\pi z}{a}\right), \tag{5}$$

for $n = 1, 3, 5 \ldots$, and

$$\phi_n(z) = c_n \left(\sin \frac{\pi z}{a}\right)^{-2\beta} \cos \frac{\pi z}{a} {}_2F_1\left(-\frac{n}{2} - 2\beta + \frac{1}{2}, \frac{n}{2} + \frac{1}{2}, \frac{3}{2}, \cos^2 \frac{\pi z}{a}\right), \tag{6}$$

for $n = 2, 4, 6 \ldots$. Here, $\beta = [(8m^*U_0a^2/\pi^2\hbar^2 + 1)^{1/2} - 1]/4$, and ${}_2F_1$ presents the confluent hypergeometric functions. The quantities c_n preferring the normalization constants which are given as follows, respectively, for the ground and first excited states: $c_1 = \pi^{1/4}[\Gamma(2\beta + 2)/a\Gamma(2\beta + 3/2)]^{1/2}$ and $c_2 = 2\sqrt{\beta + 1}c_1$. The corresponding eigenstates are [35]

$$\varepsilon_n = (n^2 + 4n\beta - 2\beta)\frac{\pi^2\hbar^2}{2m^*a^2}. \tag{7}$$

To be more convenient for further calculations, we prepare the matrix elements

$$\langle\lambda|x|\lambda'\rangle = \left[x_0\delta_{N',N} + (\alpha_B/\sqrt{2})\left(\sqrt{N}\delta_{N',N-1} + \sqrt{N+1}\delta_{N',N+1}\right)\right]\delta_{k_y',k_y}, \tag{8}$$

$$\mathcal{F}_{nn'}(\pm q_z) = \int_0^\infty e^{\pm iq_z z}\phi_n^*(z)\phi_{n'}(z)\mathrm{d}z. \tag{9}$$

3 The expression of magneto-optical absorption coefficient

To study the PACR in the above given SSQW quantum well, the expression of the MOAC is needed. This expression has been derived using the perturbative theory, which is performed as follows when the e–p interaction is included [32]

$$K(\hbar\Omega) = \frac{1}{V_0(I/\hbar\Omega)}\sum_{\lambda,\lambda'}\mathcal{W}^{\pm}_{\lambda,\lambda'}f_\lambda(1-f_{\lambda'}), \tag{10}$$

where I prefers the optical intensity with the photon energy $\hbar\Omega$, V_0 denotes the volume of the system. Also $f_{\lambda(\lambda')}$ signifies the $\lambda(\lambda')$ state's Fermi distribution function and $\mathcal{W}^{\pm}_{\lambda,\lambda'}$ is the transition matrix element. The upper (plus) sign corresponds to the emission and the lower (minus) to the absorption processes of phonon, respectively.

The summation over λ in Eq. (10) is handled using the transformation $\sum_\lambda \to \sum_{N,n}\sum_{k_y}$, in which the summation over k_y is performed using the periodic boundary conditions [36]

$$\sum_{k_y} \to \frac{L_y}{2\pi}\int_{-L_x/2\alpha_B^2}^{L_x/2\alpha_B^2} dk_y = \frac{S}{2\pi\alpha_B^2}, \tag{11}$$

where $S = L_xL_y$ denotes the system surface area, and $\alpha_B = (\hbar/m^*\omega_B)^{1/2}$ is the radius of the orbit or the magnetic length. The summation over λ' is also achieved in the same way. The overlap integral is derived from the matrix element shown in Eq. (9) as follows

$$J_{12} = \int_{-\infty}^{+\infty}\left|\mathcal{F}_{12}(\pm q_z)\right|^2 dq_z. \tag{12}$$

It is noted that, the integral over q_z in the above equation cannot be calculated exactly in the general case. However, this problem could be solved using a suggestion of Gol'dman et al. [35]. According to that, for the small values of n ($n \ll \beta$), that means we only consider the transitions between the lowest states, the eigenstates in Eq. (7) will be reduced to a simpler form as follows

$$\varepsilon_n = \frac{\hbar\pi}{a}\sqrt{\frac{2U_0}{m^*}}\left(n-\frac{1}{2}\right). \tag{13}$$

This limit is acceptable since electrons mainly occupy some lowest states. The energy spectrum described in Eq. (13) is the same as that of an oscillator with a frequency of $\omega_z = (2\pi^2U_0/m^*a^2)^{1/2}$. Using this limit, Eq. (12) yields

$$J_{12} = \frac{\pi}{2}\left(\frac{m^*U_0}{2\hbar^2a^2}\right)^{1/4}. \tag{14}$$

Then, Eq. (10) takes the following form in which the two-photon process has been included

$$K(\hbar\Omega) = C(\hbar\Omega)\sum_{N,N'}|\mathcal{B}_{\lambda\lambda'}|^2J_{12}f_{N,1}(1-f_{N',2})(P_1+P_2), \tag{15}$$

where we have denoted $\mathcal{B}_{\lambda\lambda'} = \langle\lambda|x|\lambda'\rangle$ which has been presented in Eq. (8), and

$$C(\hbar\Omega) = \frac{S^2e^4\alpha_0^2\chi^*\hbar\omega_0}{32\pi^2n_rc\int_0^2 V_0\alpha_B^6\hbar^2\Omega}, \tag{16}$$

$$P_1 = N_0^-\delta(Q_1^-) + N_0^+\delta(Q_1^+), \tag{17}$$

$$P_2 = \frac{\alpha_0^2}{8\alpha_B^2}(N+N'+1)[N_0^-\delta(Q_2^-) + N_0^+\delta(Q_2^+)], \tag{18}$$

$$Q_p^\pm = \Delta E \pm \hbar\omega_L - p\hbar\,\Omega, \quad p = 1,2, \tag{19}$$

where e is the absolute of electron charge, α_0 is the dressing parameter, $\chi^* = (1/\chi_\infty - 1/\chi_0)$ with $\chi_\infty = 10.89$ and $\chi_0 = 13.18$ being, respectively, the high- and low-frequency dielectric constants for GaAs [34], n_r denotes the refractive index, c refers to the speed of light, ϵ_0 is the permittivity of the free space, $\Delta E = E_{N',2} - E_{N,1}$ is the transition energy difference, and $N_L^\pm = N_L + 0.5 \pm 0.5$ with $N_L = [e^{\hbar\omega_L/(k_BT)} - 1]^{-1}$ being the distribution function of LO-phonon where $\hbar\omega_L = 36.25$ meV is the energy of phonon [34].

To avoid the divergent problem, in Eqs. (17) and (18), the delta functions will be transformed by the Lorentzian width $\gamma^\pm_{N'N}$ using the following relation $\delta(Q_p^\pm) = \left(\gamma^\pm_{N'N}/\pi\right)\left[(Q_p^\pm)^2 + (\gamma^\pm_{N'N})^2\right]^{-1}$, where

$$\left(\gamma^\pm_{N'N}\right)^2 = \frac{e^2\chi^*V_0\hbar\omega_L}{32\pi\epsilon_0S\alpha_c(N'-N)}\left(\frac{m^*U_0}{2\hbar^2a^2}\right)^{1/4}N_L^\pm, \tag{20}$$

where we have used the Eq. (A6) of Ref. [37].

4 Numerical results and discussion

This section is devoted to present the numerical results about the PACR effect in SSQW. To do that, we will discuss the dependence of the product $f_{0,1}(1-f_{1,2})$, the energy separation ΔE, the MOAC and the FWHM on the controlling parameters such as magnetic field, a parameter, and temperature. The characteristics used in our numerical calculations are [34, 38, 39]: $n_r = 3.2$, $\alpha_0 = 7.5$nm, and $U_0 = 228$ meV, and the electron density $n_e = 3\times10^{16}$ cm^{-3} which leads to the Fermi energy of $E_F = 0.156$ eV.

Because the intensity of MOAC is strongly changed by the factor $f_{N,1}(1-f_{N',2})$ (see Eq. (15)), to be more convenient in discussing the dependence of the MOAC's intensity on the magnetic field, the parameter a, and the temperature, in Fig. 2, the variation of the factor $f_{0,1}(1-f_{1,2})$ on magnetic field for two distinguishing values of T and a is shown. The product is shown to be decreased with the magnetic field, whereas it was increased with the parameter a. The effect of temperature on the product is more complicated due to the thermal spread: in the low magnetic region, the thermal spread makes the product reduce, whereas in the higher magnetic field one, the product enhances with temperature. The contact point occurs at $B = 12.48$ T, at which the ground state's energy level is equal to the Fermi energy level.

Note that the energy separation, ΔE, is also the principal characteristic determining the MOAC, especially the peaks' positions. It is vital to display the change of ΔE with the variation of input parameters as shown in Fig. 3. It is observed that the energy separation rises linearly when the magnetic field B increases but tends to reduce non-linearly with the enhancement of a. The linear dependence of ΔE on the B parameter is caused by the proportion to B of cyclotron energy $\hbar\omega_B$, whereas the nonlinear reduction of ΔE with a parameter results from Eq. (7), in which, ε_n is

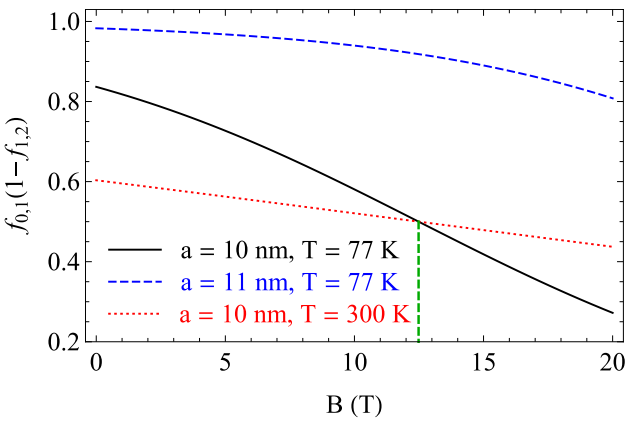

Fig. 2 The product $f_{0,1}(1-f_{1,2})$ a function of the magnetic field B

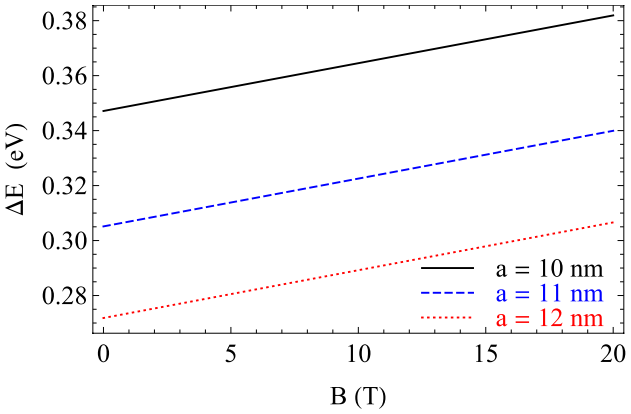

Fig. 3 Energy separation, ΔE, versus magnetic field B with three different values of a

proportional to a^{-2}. A similar result has been observed in another shape quantum well [40].

In Fig. 4, we show the MOAC as functions of photon energy for $B = 8$ T, 10 T, and 12 T. We found that there are four peaks in each curve, which are numbered sequentially from "1" to "4" for the case of $B = 8$ T, for example. They are formed by the PACR transitions, i.e., the peaks' positions satisfy the resonant conditions

$$p\hbar\Omega = \Delta E \pm \hbar\omega_L,\ (p = 1, 2). \tag{21}$$

Recall that in above equation, the plus and minus signs, respectively, correspond to the absorption and emission processes of one LO-phonon of energy $\hbar\omega_L$. For example, in the curve with $B = 8$ T (the black solid curve), two peaks labeled "1" and "3" are generated by the phonon absorption process, while two peaks "2" and "4" are caused by the emission process. It is clear that the phonon emission

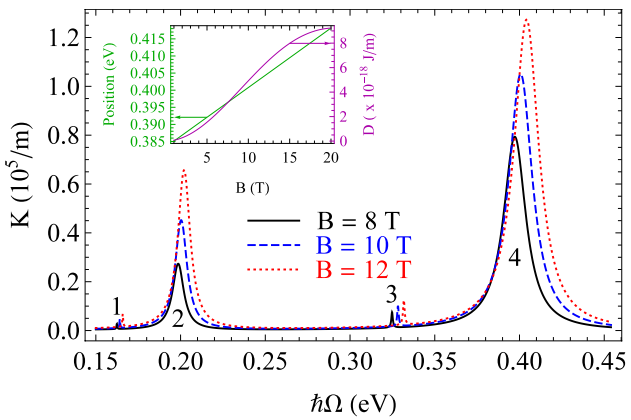

Fig. 4 The variation of MOAC as a function of photon energy $\hbar\Omega$ for distinguishing values of magnetic field at $a = 10$ nm and $T = 77$ K. The inset depicts the peaks' position (left vertical axis) and the factor $D = A(\hbar\Omega)|B_{\lambda\lambda'}|^2 J_{12} f_{0,1}(1-f_{1,2})$ (right vertical axis) due to one-photon absorption process as functions of B

process occurs much more strongly than the phonon absorption process. This result is also observed in other type shapes of quantum wells [40, 41]. In more detail, the two peaks "1" and "3" located correspondingly at $\hbar\Omega = 0.162$ eV and 0.325 eV are the consequences of the transitions of electron from the ground state to the first excited one via absorbing one photon ($p = 1$, peak "3") or two photons ($p = 2$, peak "1"). The corresponding positions of emission phonon peaks are $\hbar\Omega = 0.199$ eV ($p = 2$, peak "2") and 0.397 eV ($p = 1$, peak "4"). In both phonon absorption and emission cases, the two-photon peaks' intensities are about 43% of the one-photon peaks' ones. This rate shows the critical role of the two-photon process, which is significantly considerable in comparison with the one-photon one. For that reason, the two-photon issue should be added in studying the PACR effect in low-dimensional quantum wells.

Now we discuss the influence of magnetic field on the PACR peaks. Figure 4 depicts that the rising magnetic field gives rise to the peaks' intensities and contemporaneously pushes their positions towards the higher energies regime (blue shift). These features can be understood physically as follows: we can deduce from the Eqs. (15) and (16) that the intensities of the PACR peaks are proportional to $\alpha_B^{-6} \sim B^3$. This relationship directly results in the rise of the peaks' intensities when the B parameter increases as clearly shown in the right vertical axis of the inset. Meanwhile, the blue shift feature of the PACR spectrum is caused by the extension of energy separation with B (see Fig. 3), which is very close to the behavior of the peaks' positions shown in the left vertical axis of the inset. This is suitable because the peaks' position and the energy separation are only different by the LO-phonon energy (see Eq. (21)). The present result is very close with previous works reported in quantum wells with different potential shapes [17, 21, 22, 40, 42–46] and those reported in others low-dimensional systems as well [47–51]. Besides the cause of the blue shift and the enhancing peaks' intensities, the rise of B is also the cause of the peaks' broadening. This will be clearly illustrated in the next figure where we talk about the effect of magnetic field on the FWHM.

Because of its close relationship with the Lorentz width [see Eq. (20)], the magnetic field affects significantly the FWHM. To have a visual view of the magnetic field effect on the profile of the PACR peaks, in Fig. 5, we show the variation of FWHM with B at specific values of a and T. In all cases presented in Fig. 5, FWHM increases by magnetic field with a nonlinear law, which are in accordance with those revealed in bulk materials [25], in quantum wells with other types of potential shape [24, 40, 43], in graphene [30, 31, 52, 53], and in monolayer molybdenum disulfide [32]. Besides, we can also see that the FWHM due to the phonon emission, which is proportional to N_L^+, is larger than that due to the absorption one, which is proportional to N_L^-. This

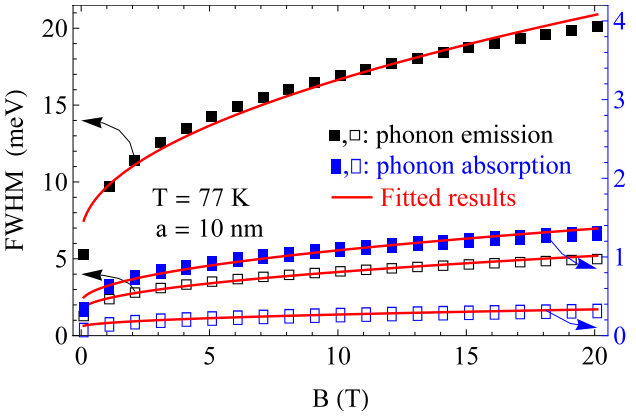

Fig. 5 Magnetic field dependence of FWHM. The full and empty symbols, respectively, refer to the one- and two-photon resonances

result implies that at the observed condition, N_L is much smaller than 1.

To have more accurate information on the effect of magnetic field, we now show the fitting expression of the FWHM in the unit of meV as follows: $\text{FWHM} = \alpha_B + \beta_B B^{1/2}$, where the magnetic field is measured in the unit of Tesla. In the case of phonon emission process, we found the best-fit values of α_B and β_B as $\alpha_B = 6.46\,(1.61)$ meV and $\beta_B = 3.22\,(0.80)$ meV for the process of one-(two-)photon. In the case of phonon absorption one, their corresponding values are $\alpha_B = 0.42\,(0.11)$ meV and $\beta_B = 0.21\,(0.05)$ meV. The obtained results are displayed by the solid curves in the Fig. 5. The square root of B-dependent FWHM observed here is comparable with that observed in other quantum wells with different types of confinement potential [40, 43, 54, 55].

To understand the effect of the a parameter on the PACR peaks, in Fig. 6, we plot the MOAC as functions of $\hbar\Omega$ for $a = 10$, 11, and 12 nm. For convenience in comparison, here we choose $B = 10$ T and $T = 77$ K, which are reported in an earlier published paper [40]. The primary trend of the effect of a parameter is that the increase of a pushes the peaks' position towards the lower energies regime (red shift) and enhances the peaks' intensities as well. The obtained results here are completely consistent with that reported in a quantum well with another confining potential shape [40]. The red shift effect is the cause of the reduction of the energy separation as shown in Fig. 3 and it is visually illustrated in the inset (left vertical axis) of Fig. 6. For the physical explanation of the peaks' intensities, note that the peaks intensities are closely related with the factor D, which is shown in the right vertical axis of the inset. It is observed that with the increase of the a parameter, the factor D first increases quickly from $a = 9$ nm, touches its maximum at $a = 11.5$ nm, and then gradually reduces if the a parameter increases further. This behavior of the D factor directly

Table 1 The results of the defined parameters σ_1, σ_2 and σ_3

Parameters	Line (*a*)	Line (*b*)	Line (*c*)	Line (*d*)
σ_1 (meV)	15.46	1.00	3.85	0.24
σ_2 (meV nm^{-1})	− 0.12	− 0.007	− 0.03	− 0.002
σ_3 (meV nm)	26.00	1.84	6.69	0.57

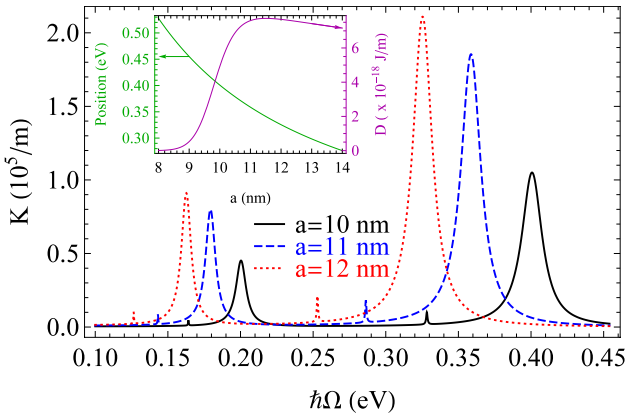

Fig. 6 The variation of MOAC as a function of photon energy $\hbar\Omega$ for distinguishing values of a at $B = 10$ T and $T = 77$ K. The inset depicts the peaks' position (left vertical axis) and the factor $D = A(\hbar\Omega)|B_{\lambda\lambda'}|^2 J_{12} f_{0,1}(1 - f_{1,2})$ (right vertical axis) due to one-photon absorption process as functions of B

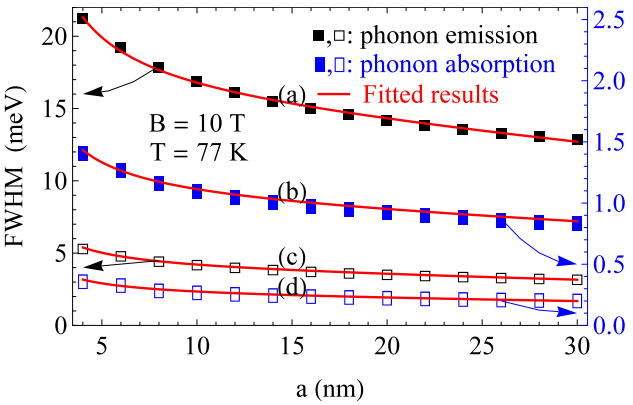

Fig. 7 a-parameter dependence of FWHM. The full and empty symbols, respectively, refer to the one- and two-photon resonances

explains the increasing feature of the peaks' intensities when the a parameter increases from 10 nm to 11 nm and then to 12 nm.

Beside the effect on the resonant peaks' positions and intensities as shown in Fig. 6, the a parameter also influences the FWHM. In Fig. 7, we show the a-dependent FWHM. The results are calculated for either both phonon processes or both photon absorption ones. All four cases show a reduction of the FWHM with the increasing a. It means that the

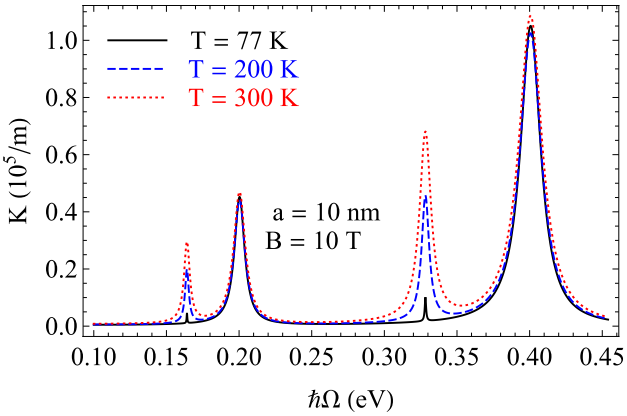

Fig. 8 The variation of MOAC as a function of photon energy $\hbar\Omega$ for distinguishing values of temperature

bigger the value of a parameter is, the weaker the quantum confinement effect is, and therefore the reduction of the e–p scattering. Besides, similar to that in quantum well with other shapes [40, 41], here we also observe in the SSQW that the contribution to FWHM of phonon absorption is much smaller than that of other process. This result is clearly manifested through the scale of vertical axes of the Fig. 7.

To have a quantitative result about the a-dependent FWHM, we suggest a fitted expression as follows: FWHM (meV)$= \sigma_1 + \sigma_2 a + \sigma_3 a^{-1}$, where σ_1, σ_2, and σ_2 are the defined parameters, which are listed in the Table 1. The obtained results are shown by the solid curves in Fig. 7. To our knowledge, these results are new, and it is necessary to have an experimental work to test their validity.

It is seen from Eq. (15) that the temperature influences on the PACR effect through only the factor $f_{N,1}(1 - f_{N',2})$ and the phonon population N_L. This means that the temperature affects only the peaks' intensities but does not affect the peaks' positions, as shown plainly in Fig. 8, in which we display MOAC as functions of $\hbar\Omega$ for $T = 77$ K, 200 K, and 300 K at $a = 10$ nm and $B = 10$ T. It is clear that with the increase of T, the peaks' intensities are raised while their positions are maintained. The results obtained here are in accordance with those available in published works [40, 43, 46]. Besides, there is a crucial feature here, that is the temperature negligibly affects the resonant peaks caused by the phonon emission (the second and the fourth peaks) but strongly affects those generated by the phonon absorption process (the first and the third peaks). This result agrees with that reported in quantum wells with different confining potential shapes [40, 41]. It is noticed that although the temperature does not affect the peaks' positions, it changes the peaks' widths or FWHM as shown in the following figure.

In Fig. 9, we depict the FWHM as functions of temperature at a fixed value of B and a. The results are reported for both cases of phonon process: either emission

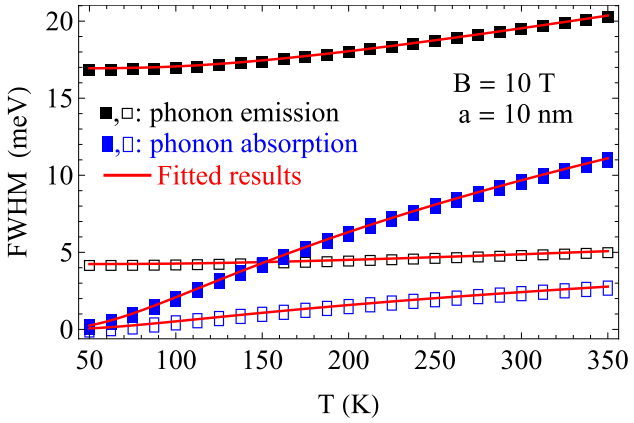

Fig. 9 Temperature dependence of FWHM. The full and empty symbols, respectively, refer to the one- and two-photon resonances

or absorption ones. In each case of phonon process, the results are calculated for both means of the photon: one- and two-photon ones. It means that we have four different cases in the total, corresponding to four different lines in Fig. 9. We found that the FWHM enhances as an increasing function of temperature in both cases of phonon but with the different rules: while the FWHM due to phonon emission process is proportional to N_L, the corresponding principle due to the phonon absorption one is $N_L^{1/2}$. In more detail, we can express the fitted expression of FWHM (in the unit of meV) for the phonon emission process as follows [56, 57]:

$$\text{FWHM} = \alpha_T + \beta_T N_L, \tag{22}$$

where α_T and β_T correspond to the stable and thermal broadening terms of FWHM, respectively. With the help of the formula $N_L = [e^{\hbar\omega_L/(k_B T)} - 1]^{-1}$, we find the best-fit values of α_T and β_T as follows for the one- (two-) photon process $\alpha_T = 16.94\,(4.24)\,\text{meV}$ and $\beta_T = 7.94\,(1.94)\,\text{meV}$, respectively. In Fig. 9, the fitted results are displayed by the solid red curves, which show that the analytical expression in Eq. (22) fits perfectly with results obtained by numerical calculation (the square dots). Besides, the obtained values of α_T and β_T here are more significant than those calculated analytically in the quantum well with other confining potential shapes [43] as well as the experimental results in multiple quantum well structures [56, 57].

Finally, for the phonon absorption process, the result corresponding to Eq. (22) is: $\text{FWHM} = \gamma_T N_L^{1/2}$, where the fitted factor γ_T is found as follows: $\gamma_T = 16.91\,\text{meV}$ and $\gamma_T = 4.23\,\text{meV}$ correspond to the absorption processes of one- and two-photon, respectively. To the best of our knowledge, this result is new, and it should be tested by further experiments.

5 Conclusion

We have discussed theoretically in detail the effects of magnetic field, well parameter, and temperature on the PACR in a SSQW by studying the energy separation, the MOAC, and the FWHM. The results showed that while the magnetic field and the well parameter, a, affect the energy separation, the MOAC, and the FWHM strongly, the temperature only influences the MOACs peaks' intensities but does not change the energy separation and the peaks' positions. In detail, the energy separation rises linearly with the magnetic field but reduces non-linearly with the well parameter. The MOAC peaks show a blue shift behavior with the increase of magnetic field, changes to lower energy region with the increase in the a parameter, but maintains the changing temperature. The FWHM is found to rise with magnetic field and temperature, but reduces with the well parameter, in which the thermal broadening mechanism of the FWHM due to the phonon emission process fits well with the experimental observation in multiple quantum well structures.

We also found that the FWHM varies in all cases (phonon emission and absorption as well as one- and two-photon absorption) as $\text{FWHM}\,(\text{meV}) = \sigma_1 + \sigma_2 a + \sigma_3 a^{-1}$, whereas in the phonon absorption process as $\text{FWHM} = \gamma_T N_L^{1/2}$. The dependence of the FWHM on the a parameter and the temperature has been obtained in the special asymmetric hyperbolic-type quantum well as well [40]. To the best of our knowledge, these results are new, and it is necessary to perform further studies to examine its validity.

Compliance with ethical standards

Conflict of interest The authors declare that they have no conflicts of interest.

References

1. W. Xu, F.M. Peeters, J.T. Devreese, J. Phys. Condens. Matter **5**, 2307 (1993)
2. X.L. Lei, Phys. Rev. B **77**, 205309 (2008)
3. T.C. Phong, L.T. Thu Phuong, H.V. Phuc, P.T. Vinh, J. Korean Phys. Soc. **62**, 305 (2013)
4. L.T.T. Phuong, H.V. Phuc, T.C. Phong, Phys. E **56**, 102 (2014)
5. G. Dresselhaus, A.F. Kip, C. Kittel, Phys. Rev. **98**, 368 (1955)
6. J.M. Luttinger, Phys. Rev. **102**, 1030 (1956)
7. R.N. Dexter, H.J. Zeiger, B. Lax, Phys. Rev. **104**, 637 (1956)
8. P. Warmenbol, F.M. Peeters, J.T. Devreese, Phys. Rev. B **37**, 4694 (1988)
9. F.M. Peeters, J.T. Devreese, Semicond. Sci. Technol. **7**, B15 (1992)
10. T.C. Phong, L.T.T. Phuong, N.D. Hien, V.T. Lam, Phys. E **71**, 79 (2015)

11. E.J. Johnson, D.H. Dickey, Phys. Rev. B **1**, 2676 (1970)
12. Y.H. Matsuda, T. Ikaida, N. Miura, S. Kuroda, F. Takano, K. Takita, Phys. Rev. B **65**, 115202 (2002)
13. K. Rachor, T.E. Raab, D. Heitmann, C. Gerl, W. Wegscheider, Phys. Rev. B **79**, 125417 (2009)
14. Y.B. Yu, K.X. Guo, S.N. Zhu, Phys. E **27**, 62 (2005)
15. Y.B. Yu, S.N. Zhu, K.X. Guo, Solid State Commun. **139**, 76 (2006)
16. R. Khordad, H. Bahramiyan, Superlattices Microstruct. **76**, 163 (2014)
17. J.S. Bhat, S.S. Kubakaddi, B.G. Mulimani, J. Appl. Phys. **70**, 2216 (1991)
18. M. Singh, B. Tanatar, Phys. Rev. B **41**, 12781 (1990)
19. B. Tanatar, M. Singh, Phys. Rev. B **42**, 3077 (1990)
20. M.W. Goodwin, D.G. Seiler, Phys. Rev. B **27**, 3451 (1983)
21. J.S. Bhat, B.G. Mulimani, S.S. Kubakaddi, Phys. Rev. B **49**, 16459 (1994)
22. J.S. Bhat, R.A. Nesargi, B.G. Mulimani, Phys. Rev. B **73**, 235351 (2006)
23. N. Shon, T. Ando, J. Phys. Soc. Jpn. **67**, 2421 (1998)
24. M.P. Chaubey, C.M. Van Vliet, Phys. Rev. B **34**, 3932 (1986)
25. J.Y. Sug, S.G. Jo, J. Kim, J.H. Lee, S.D. Choi, Phys. Rev. B **64**, 235210 (2001)
26. H.V. Phuc, L.V. Tung, P.T. Vinh, L. Dinh, Superlattices Microstruct. **77**, 267 (2015)
27. Z. Jiang, E.A. Henriksen, L.C. Tung, Y.J. Wang, M.E. Schwartz, M.Y. Han, P. Kim, H.L. Stormer, Phys. Rev. Lett. **98**, 197403 (2007)
28. G. Li, A. Luican, E.Y. Andrei, Phys. Rev. Lett. **102**, 176804 (2009)
29. M. Orlita, C. Faugeras, P. Plochocka, P. Neugebauer, G. Martinez, D.K. Maude, A.L. Barra, M. Sprinkle, C. Berger, W.A. de Heer, M. Potemski, Phys. Rev. Lett. **101**, 267601 (2008)
30. H.V. Phuc, N.N. Hieu, Opt. Commun. **344**, 12 (2015)
31. B.D. Hoi, L.T.T. Phuong, T.C. Phong, J. Appl. Phys. **123**, 094303 (2018)
32. C.V. Nguyen, N.N. Hieu, N.A. Poklonski, V.V. Ilyasov, L. Dinh, T.C. Phong, L.V. Tung, H.V. Phuc, Phys. Rev. B **96**, 125411 (2017)
33. T.C. Phong, H.V. Phuc, Mod. Phys. Lett. B **25**, 1003 (2011)
34. S. Adachi, J. Appl. Phys. **58**, R1 (1985)
35. I.I. Gol'dman, V.D. Krivchenkov, V.I. Kogan, V.M. Galitskii, *Problems in Quantum Mechanics* (Inforsearch, London, 1960)
36. P. Vasilopoulos, Phys. Rev. B **33**, 8587 (1986)
37. M.P. Chaubey, C.M. Van Vliet, Phys. Rev. B **33**, 5617 (1986)
38. E. Li, Phys. E **5**, 215 (2000)
39. F. Ungan, U. Yesilgul, S. Sakiroglu, M.E. Mora-Ramos, C.A. Duque, E. Kasapoglu, H. Sari, I. Sökmen, Opt. Commun. **309**, 158 (2013)
40. K.D. Pham, L. Dinh, P.T. Vinh, C.A. Duque, H.V. Phuc, C.V. Nguyen, Superlattices Microstruct. **120**, 738 (2018)
41. H.V. Phuc, D.Q. Khoa, N.V. Hieu, N.N. Hieu, Optik **127**(22), 10519 (2016)
42. H.V. Phuc, N.D. Hien, L. Dinh, T.C. Phong, Superlattices Microstruct. **94**, 51 (2016)
43. L.V. Tung, P.T. Vinh, H.V. Phuc, Phys. B **539**, 117 (2018)
44. E. Ozturk, I. Sökmen, J. Lumin. **145**, 387 (2014)
45. H. Sari, E. Kasapoglu, S. Sakiroglu, U. Yesilgul, F. Ungan, I. Sökmen, Phys. E **90**, 214 (2017)
46. L.V. Tung, P.T. Vinh, L. Dinh, H.V. Phuc, Int. J. Mod. Phys. B **32**, 1850162 (2018)
47. Y. Karaaslan, B. Gisi, S. Sakiroglu, E. Kasapoglu, H. Sari, I. Sökmen, Superlattices Microstruct. **93**, 32 (2016)
48. G. Liu, K. Guo, C. Wang, Phys. B **407**(12), 2334 (2012)
49. G. Liu, K. Guo, H. Hassanabadi, L. Lu, Phys. B **407**, 3676 (2012)
50. C.M. Duque, A.L. Morales, M.E. Mora-Ramos, C.A. Duque, J. Lumin. **143**, 81 (2013)
51. E.C. Niculescu, D. Bejan, Philos. Mag. **97**, 2089 (2017)
52. H.V. Phuc, L. Dinh, Mater. Chem. Phys. **163**, 116 (2015)
53. H.V. Phuc, Superlattices Microstruct. **88**, 518 (2015)
54. H.V. Phuc, N.T.T. Thao, L. Dinh, T.C. Phong, J. Phys. Chem. Solids **75**, 300 (2014)
55. H.V. Phuc, J. Phys. Chem. Solids **82**, 36 (2015)
56. D.A.B. Miller, D.S. Chemla, D.J. Eilenberger, P.W. Smith, A.C. Gossard, W.T. Tsang, Appl. Phys. Lett. **41**, 679 (1982)
57. D. Gammon, S. Rudin, T.L. Reinecke, D.S. Katzer, C.S. Kyono, Phys. Rev. B **51**, 16785 (1995)